Characterization of the developing lacuno-canalicular network during fracture repair

Michele Casanova[1], Aaron Schindeler[2,3§], Lauren Peacock[2], Lucinda Lee[2,3], Philipp Schneider[1,4,5], David G Little[2,3], Ralph Müller[1]

[1] Institute for Biomechanics, ETH Zurich, Zurich, Switzerland

[2] Orthopaedic Research & Biotechnology, The Children's Hospital at Westmead, Westmead, Australia

[3] Discipline of Child and Adolescent Health, University of Sydney, Camperdown, Australia

[4] Bioengineering Science Research Group, Faculty of Engineering and Physical Sciences, University of Southampton, Southampton, UK

[5]High-Performance Vision Systems, Center for Vision, Automation & Control, AIT Austrian Institute of Technology, Vienna, Austria

§ Contact Author

A/Prof Aaron Schindeler (aaron.schindeler@sydney.edu.au)

Bioengineering & Molecular Medicine Laboratory

The Children's Hospital at Westmead

Locked Bag 4001

Westmead, NSW 2145

Australia

Abstract: Fracture repair is a normal physiological response to bone injury. During the process of bony callus formation, a lacuno-canalicular network (LCN) is formed *de novo* that evolves with callus remodeling. Our aim was the longitudinal assessment of the development and evolution of the LCN during fracture repair. To this end, 45 adult wild type C57BL/6 mice underwent closed tibial fracture surgery. Fractured and intact contralateral tibiae were harvested after 2, 3, and 6 weeks of bone healing (n=15/group). High-resolution micro-computed tomography (μCT) and deconvolution microscopy (DV) approaches were applied to quantify lacunar number density from the calluses and intact bone. On histological sections, Goldner's trichrome staining was used to assess lacunar occupancy, fluorescein isothiocyanate staining to visualize the canalicular network, and TUNEL staining to examine osteocyte apoptosis. Analysis of μCT scans showed progressive decreases in mean lacuna volume over time (-27% 2-3 weeks, -13% 3-6 weeks). Lacunar number density increased considerably between 2 and 3 weeks (+156%). Correlation analysis was performed, showing a positive linear relationship between canalicular number density and

trabecular thickness (R^2=0.56, p<0.001) and an inverse relationship between mean lacuna volume and trabecular thickness (R^2=0.57, p<0.001). Histology showed increases in canalicular number density over time (+22% 2-3 weeks, +51% 3-6 weeks). Lacunar occupancy in new bone of the callus was high (>90%), but the old cortical bone within the fracture site appeared necrotic as it underwent resorption. In conclusion, our data shows a progressive increase in the complexity of the LCN over time during fracture healing and demonstrates that this network is initiated during the early stages of repair. Further studies are needed to address the functional importance of osteocytes in bone healing, particularly in detecting and translating the effects of micromotion in the fracture.

Keywords: Fracture repair; bone quality; canaliculi, osteocyte lacunae, lacuno-canalicular network; micro-computed tomography

Introduction

Osteocytes are bone cells buried within the bone matrix that act as mechanotransducers [(1)] and orchestrate bone remodeling [(2)]. They communicate with each other via the lacuno-canalicular network (LCN), which is critical for regulating bone homeostasis [(2)]. The LCN has been recently shown to play a major role in the spatial distribution of mass density (i.e. mineralization level) in bone [(3,4)] and acts to modulate bone mineral based on paracrine and hormonal factors [(5,6)].

As the LCN has a key role in modulating deposition, absorption, and mineralization of bone, it fundamentally influences the biomechanics of the bone matrix. Multiple studies have shown that osteocyte number density can be positively correlated with bone biomechanical properties and its resistance to fracture [(7-10)]. In fact, both lacunar number density and mean lacuna volume are correlated with the propagation of microcracks [(11-13)]. It is established that lacunae can act as force concentrators [(14)], and can lead to bone fragility in poorly ordered bone structures [(15)]. Furthermore, changes in the organization of canaliculi have been suggested to affect the mechanical properties of bone [(16-18)].

During fracture repair, new woven bone is produced to bridge the fracture gap, and within this regenerating hard callus tissue a new LCN is required to form *de novo*. The importance of the forming LCN within bone healing has been a subject for recent discussion [(19)], and may have a central role in determining callus size [(20,21)]. Micromotion has been shown to be important for fracture healing, while overly rigid fixation can lead to stress shielding and insufficient new bone formation, which may be monitored by the nascent LCN.

In this preclinical study, we aimed to investigate how lacunar measures and canalicular number density evolve during fracture repair. We hypothesized that lacunar number and canalicular number density would change longitudinally during bone healing. Prior work demonstrated the formation of the LCN during bone healing and examined pharmacological modulation of the LCN, but these studies were limited to a single time point [22]. Analysis was performed to investigate whether callus macro- and microarchitecture could be correlated to lacunar measures or canalicular number density, since these factors are related to bone deposition and structure in intact bone [20,23-25]. While lacunar number density can be derived from μCT imaging, lacunar occupancy required further histological analysis. In particular, the presence of apoptotic osteocytes could possibly initiate perilacunar osteolysis and localized bone destruction [23,26].

On these grounds, we investigated the LCN development at three time points during murine bone fracture repair. Following closed tibial fracture surgery, the LCN was characterized using morphometric measures at 2, 3 and 6-week time points after fracture. These represent distinct phases of the bone healing process. Two weeks represents an early stage of fracture repair, where the callus is mostly cartilaginous and the LCN is starting to be formed. Three weeks presents a consolidated callus, which is mostly mineralized and also around its peak in bone volume. Six weeks denotes a callus that is finalizing remodeling towards the original bone shape.

This study also features innovations in examining the LCN network. In prior studies, quantification of the LCN has been restricted to small regions encompassing a limited number of osteocyte lacunae and/or osteocytes [27]. In this study, we have used an advanced approach combining deconvolution microscopy (DV) and high-resolution micro-computed tomography (μCT) [28]. This enabled us to quantify large regions from the central portion of the calluses, providing a broader overview on the LCN development in bone fracture repair. μCT was also performed on the whole calluses at lower spatial resolutions to compute tissue mineral density, bone volume fraction and micro-architectural measures. Goldner's trichrome stain was performed on a subset of histological sample sections to assess lacunar occupancy and a TUNEL stain was used to examine apoptosis. Together, these imaging modalities reveal a complex picture of the longitudinal changes in the LCN that occur over time during fracture healing.

Materials and Methods

Animals and surgery

Forty-five female, 11-week-old wild type mice (C57BL/6) were used in this study. All animals underwent a closed fracture on their right tibia using an established fracture protocol [29]. In brief, animals were anaesthetized with ketamine and xylazine and a complete fracture made without

breaking the skin using a handheld device made from surgical staple removers. Fractures were fixed via the intramedullary canal with solid stainless-steel insect pins inserted via the knee. Fractures were confirmed using X-ray radiography and animals were monitored by weekly X-ray radiographies during the fracture healing process (Faxitron MX-20, Wheeling IL, USA). Animals were given buprenorphine (0.05 mg/kg) for analgesia up to every 12 hours as required. Fractured mice were subsequently harvested at three different time points (n=15 per time point). Group 1 was harvested 2 weeks after fracture, Group 2 after 3 weeks, and Group 3 after 6 weeks. All animal experiments were approved by the Westmead Hospital Animal Ethics Committee.

Specimen collection

Fractured and contralateral tibiae were extracted and fixed in 4% phosphate-buffered formalin overnight at 4°C. After fixation, the samples were immersed in 30% sucrose solution for a day, then snap frozen in OCT medium (TissueTek OCT Compound, Thermo Fisher Scientific, Hampton NH, USA) and cryosectioned (Leica CM1950, Wetzlar, Germany). The bones were cut in the sagittal plane, starting from the medial side. Sections of 5, 7, and 20 µm thickness were cut close to the central portion, paying attention to conserve the lateral part of the callus intact for subsequent µCT. Sections were taken using cryofilm to preserve the intact bone (SECTION-LAB Co. Ltd. Hiroshima, Japan). The cryofilm sections were adhered to glass microscope slides using a chitosan adhesive [1% Chitosan (MilliporeSigma, St. Louis, MO, USA) in 0.25% acetic acid] and left to dry at 4°C overnight.

Micro-computed tomography (µCT)

µCT scans and morphometric analyses were performed according to published methods for the assessment of bone microstructure using µCT [30]. To investigate lacunar number density and mean lacuna volume, all lateral portions of the 90 samples were scanned using a µCT system (µCT 50; Scanco Medical, Brüttisellen, Switzerland). Only lateral portions could be scanned since samples were cryosectioned after extraction (see previous section). A stack with a height of 1.1 mm was acquired from the central portion of the calluses and from the non-fractured tibiae at 45% of the tibial length starting distally. An isotropic voxel size of 1.2 µm, a tube voltage of 70 kVp, an X-ray intensity of 57 µA and an integration time of 1.5 s were selected. A Gaussian filter (sigma=0.8, support=1.0) was applied for noise reduction. Old bone and newly formed bone were segmented using customized IPL file scripts (Image Processing Language; Scanco Medical, Brüttisellen, Switzerland). Lacunar number density (defined as number of lacunae to bone volume + lacunar

porosities) and mean lacuna volume (defined as total lacunar volume divided by number of lacunae) were inferred from both old and newly formed bone.

To assess callus bone volume fraction, tissue mineral density (TMD), and micro-architectural measures, all bone calluses were scanned again including all new formed bone using µCT. An isotropic voxel size of 7 µm, a tube voltage of 55 kVp, an X-ray intensity of 72 µA, and an integration time of 1.5 s were set. A Gaussian filter (sigma=0.8, support=1.0) was applied for noise reduction. We then used IPL to manually segment the newly formed bone, excluding the bone in the intramedullary canal. Regions in which the porosity was inferior to 50% of the local total volume were considered dense woven bone and excluded for further analysis. Bone volume fraction was then assessed in these sub-volumes (macro-architectural measure). For computing the micro-architectural measures, the microstructure of the mineralized struts of the calluses was then isolated from the dense woven bone. A bone callus of the 6 weeks post-operative (post-op) group was removed from the subsequent computations for the absence of a significant quantity of struts (sample towards the end of the remodeling phase). Trabecular number (Tb.N), trabecular thickness (Tb.Th), trabecular separation (Tb.Sp), standard deviation of Tb.Th (Tb.Th.SD), standard deviation of Tb.Sp (Tb.Sp.SD), degree of anisotropy (DA), connectivity density (Conn.D) and the structure model index (SMI) were then computed as described by Bouxsein et al. [30].

Canalicular number density

Four 20-µm-thick sections of each sample were used to investigate canalicular number density. The samples were dehydrated, then covered with a 1% fluorescein isothiocyanate (FITC) solution in absolute alcohol and left overnight at 4°C. The samples were mounted and coverslipped, then analyzed using a deconvolution microscope (Deltavision, Isaquah, WA, USA). Datasets of 60 stacks with a thickness of 0.2 µm and a magnification of 60× were acquired. In each of the 90 samples, the cell processes of 10 to 12 osteocytes were examined. The osteocytes analyzed were in the central portion of the calluses and in intact tibiae at the 45% of the tibial length starting distally, which corresponds to the height where the fracture was created in the opposite tibia (fractured tibia). To estimate canalicular number density, a region of interest (ROI) was defined by contouring the lacuna on the optical section with its largest visible area. Since osteocyte processes fan out radially, the upper limit of the imaged ROI was then translated ~1 µm above the cell body. The canaliculi in the ROI were then manually counted using ImageJ (U.S. National Institutes of Health Bethesda, MD, USA) and reported relative to the ROI size to calculate the 2D canalicular density. To facilitate their identification, edge enhancement and absolute thresholding of the images was performed.

Lacunar occupancy and histological assessment

Two 5-µm-thick sections from five fractured tibiae per group and their respective contralateral bones were stained with Goldner's trichrome. Osteocyte occupancy was assessed in both newly formed and intact bone. To determine osteocyte occupancy, 10 sub-regions covering a total bone area of 1 mm^2 were selected for each sample. The sub-regions were sampled from the central portion of the calluses and on the cortical bone of the intact tibiae at the 45% of the tibial length starting distally. Empty lacunae were defined as lacunae without any visible remnant of cellular material. To prevent false negatives, only lacunae with a visible cross-section of at least 16 μm^2 were considered in the assessment.

A 7-µm-thick tibial fracture section from each mouse in each group (n=15) was stained using the DeadEnd™ Colorimetric TUNEL System (Promega Corporation, Madison, WI, USA) to label apoptotic cells in the fracture callus with DAB. The standard protocol for this kit was followed. Tissue sections were counterstained with Harris' hematoxylin (POCD Scientific, North Rocks, Australia), mounted with Aquatex (Merck Group, Darmstadt, Germany) and coverslipped for imaging on an Aperio Scanscope brightfield slide scanner (Leica Biosystems, Mt Waverley, Australia) using the 40× objective. Representative images from each group were selected.

Statistical analysis

All statistical analyses were performed using SPSS Statistics (version 20; IBM, Armonk, NY, USA). Mean and standard deviation (SD) were given for all the results. One-way ANOVA with Bonferroni *post-hoc* test was used for the analysis comparing the three groups representing different stage of bone fracture repair. For comparisons between bone calluses and intact tibiae, paired Student's *t*-tests were performed. For investigating possible correlations between morphometric measures, Pearson product-moment and quadratic correlation coefficients were computed. Paired Student's *t*-tests were used for the comparisons between mean lacuna volume of necrotic bone and of intact tibiae in the three different time points. For all analyses, $p \leq 0.05$ was considered to indicate statistical significance.

Results

Animals and surgery

No unexpected or adverse events occurred during the surgery procedure nor during post-operative monitoring. No specimens were excluded from analysis.

Micro-computed tomography (μCT)

Bone volume fraction, tissue mineral density, micro-architectural measures, and lacunar measures were estimated for the callus region at 2 weeks, 3 weeks and 6 weeks post-operatively and compared with intact contralateral bone (Table 1). This well-described fracture model [29] shows endochondral ossification of the soft callus at ~2 weeks, robust woven bone callus at ~3 weeks, and substantive new cortical bone remodeling by ~6 weeks. As healing progresses, the fracture restores itself to resemble the contralateral non-fractured bone.

Representative details of binarized high-resolution μCT scans for each group and representative three-dimensional renderings of the calluses for each group are presented in Figure 1. Mean lacuna volume significantly decreased by 27% from 2 weeks to 3 weeks post-op ($p<0.001$). Between 3 and 6 weeks post-op, the decrease was only 13% ($p<0.05$). Lacunar number density was found to be relatively low at 2 weeks, but significantly increased by 156% at 3 weeks ($p<0.001$) before decreasing by 18% ($p<0.05$) at 6 weeks. A paired Student's *t*-test detected a significant lower lacunar number density in the 6 weeks' calluses compared to their respective contralateral tibiae.

To investigate if LCN morphology is linked to the architecture of the callus, correlations (linear, quadratic, cubic) between macro- and micro-architectural measures and LCN measures (canalicular number density, lacunar number density, mean lacuna volume) were calculated within the group and versus all groups pooled. Relationships between calluses and intact tibiae were also analyzed. Table 2 presents the results of the linear correlation analysis, and statistically significant correlations were observed when data from all time points were pooled (Figure 2). In the early stages of the callus development, mean lacuna volume has a high relative standard deviation, but a constant trabecular thickness; in a later stage of fracture repair, lacuna volume is relatively stable around 320 μm^3, but trabecular thickness varies considerably.

Canalicular number density, lacunar occupancy and osteocyte apoptosis

Representative images for canalicular number density are shown in Figure 3. At all stages of callus formation and remodeling, canalicular number density was less than that seen in intact bone yet increasing over time. The results for canalicular number density are presented in Table 1. Paired Student's *t*-tests revealed statistically significant differences ($p<0.001$) between calluses and contralateral tibiae for all three time points. Analysis of the calluses between the different time points by one-way ANOVA showed a significant difference. Post-hoc analysis revealed a +22% increase in canalicular number density ($p<0.05$) between weeks 2 and 3. There was a +51% increase in canalicular number density ($p<0.001$) between weeks 3 and 6.

TUNEL staining showed a very low level of apoptotic cells at all time points (Figure 4). No apoptotic cells were observed in the parosteal cortex adjacent to the callus. Within the callus itself, few apoptotic cells were noted and were consistent with non-bone cells in the marrow space rather than osteoblasts/osteocytes. The tissue section quality was poorer in thin sections featuring regions of necrotic bone compared to the thicker sections used for quantification of the canaliculi.

Lacunar occupancy was high in the new callus and the old intact cortical bone of the tibia (Figures 5a, 5b, respectively), exceeding 90%. No significant difference in lacunar occupancy was detected, neither between the time points nor between calluses and intact bones. Within the callus some regions of old fractured cortical bone were present and showed evidence of necrosis and loss of lacunar occupancy (Figure 5c). No remnant cellular material was visible. These regions were further analyzed.

Characterization of resorbing old cortical bone

From the sections stained with Goldner's trichrome, regions corresponding to the old cortex were identified as having empty osteocyte lacunae (i.e. 0% lacunar occupancy). These areas were regions selected from 10-11 of the higher resolution μCT scans (1.2 μm voxel size) of the calluses per group and contained at least 100 lacunae. To confirm that the regions considered were not from new bone deposition, TMD (excluding canals and lacunar porosities) of the sub-volumes was compared to TMD of the scans of the intact tibiae. A plot of TMD of necrotic bone of the three groups and all contralateral tibiae showed no statistically significant difference between TMD of the calluses and TMD of the intact tibiae (Figure 6). Comparisons between mean lacuna volume of necrotic bone and of intact tibiae in the three different groups showed significant differences in mean lacuna volume between regions with necrotic cortical bone in the calluses and the intact tibiae 2 weeks post-op (+20%, $p<0.05$) and 3 weeks post-op (+27%, $p<0.001$) (Figure 6).

Discussion

μCT is a versatile imaging technique that has become the gold standard for preclinical bone analysis. Historically, the quality of μCT images precluded the analysis of osteocyte lacuna, however improvements seen with μCT enable osteocyte lacuna to be visualized. Other groups have highlighted technical advances in μCT imaging in bone in recent years. Longitudinal μCT has been performed to capture the healing process of bone healing [31], however *in vivo* imaging systems typically have far poorer spatial resolutions than those used with harvested specimens, mainly due the limited X-ray dose employed for the animals scanned *in vivo*.

While hardware capabilities have a considerable impact on the data that can be collected by μCT, the importance of software and computational analysis is often under-rated. In this study, we used a Gaussian filter to remove noise and used custom scripts to identify mineralized bone. For some quantitative analysis, manual segmentation was performed as automated segmentation of fractures can be particularly challenging. While there have been efforts to develop programs that enable accurate automated μCT segmentation [32], to date they remain less accurate than manual approaches.

μCT can increase in power when combined with other scanning and analysis modalities. For example, prior studies have attempted to combine μCT with laser Doppler to characterize neovascularization in healing fractures [33]. Our results present comprehensive snap-shots of LCN development in a quantitative fashion and were enabled by histological analysis combined with deconvolution microscopy/μCT. Our imaging process with DV microscopy offered an excellent lateral resolution, nevertheless axial resolution did not allow us to precisely quantify canalicular expression in radial direction. Thus, canalicular number density was computed on the longitudinal plane of the bone. In cortical bone of the mouse femur, canalicular number density has been shown to be higher in radial direction than in tangential direction [34].

This paper's findings are consistent with genetically modified mouse models that examine osteocytes and osteocyte gene expression in the callus. For example, conditional deletion of *Igf1* using a *Dmp1-cre* transgene accelerated bony union in mice [35]. This and other publications employing osteocyte-targeted knockout models have implied a key role for osteocyte signaling within callus. However, these studies must be interpreted within the context of off-target gene deletion by *Dmp1-cre* in other cell lineages as detected using more sensitive reporters [36]. Hence, our study showing the temporal development of the LCN will be useful for clarifying prior genetic mouse models.

This study identified two types of bone within the callus region. Firstly, there was the new mineralization of the woven bone callus that rapidly establishes an LCN. Correlation analysis indicates that this network grows in complexity as the callus remodels and while the osteocyte lacuna decreases in size, the occupancy remains high. In contrast, the bone of the former cortex become necrotic, typified by a loss of osteocytes, and will resorb over time as the new cortex forms. New bone versus old bone was also represented by an increased tissue mineral density in the old cortex. By 6 weeks, the fracture callus was highly remodeled.

This study has several limitations. While it assessed several time points, there is a fundamental variability in the fracture healing process such that some fractures may progress faster than others. Still, this is superior to prior studies by our group that examined on a single time point [22]. Group

sizes were suitable for assessing most of the primary outcome measures by μCT, but it is likely underpowered for inter-group (time point) linear correlation analysis. Nevertheless, when groups were pooled, statistically significant correlations were observed. Finally, threshold selection was determined based on arbitrary density cut-offs and thus lacuna volume and lacunar number density data should be considered in terms of differences between groups and changes over time, rather than as empirical values. Variations in mineral density in the different portion of the calcified callus encouraged us to try a gradient-threshold edge detection method, however this was unable to produce consistent results.

From a biological standpoint, the formation of the LCN is likely mediated by enzymatic degradation of the bone matrix by matrix metalloproteases (MMPs). MMP2 is necessary for LCN formation based on the reported knockout mouse phenotype [37] and critical for fracture remodeling [38]. MMP-9 knockout mice show impaired fracture repair, but the LCN was not specifically examined in this model [39]. MMP-13 is needed for peri-lacunar remodeling as well as maintaining a normal canalicular network [40], yet its role in fracture repair remains unclear.

Further research will be needed to assess the functional importance of MMPs as well as other factors expressed by osteocytes. Osteocytes express a range of important regulatory secreted proteins, such as *Sclerostin* and *RankL,* which modulate local bone formation and resorption. Thus, osteocytes and their secretome may be important for the regulation of the fracture healing process. Use of preclinical models that modulate the LCN using drugs [22] or genetic manipulation will enable the role of the LCN to be more clearly elucidated. The interaction between the nascent LCN and revascularization or bone biomechanics are also areas where there is scope for future studies. Deficiencies in blood supply are associated with impaired bone healing. Loss of stability during fracture healing can result in abundant bony callus formation with impaired union (i.e. hypertrophic non-union), and it is possible that the LCN may be critical for detecting stability and transducing signals.

In conclusion, this study is the first to present a detailed analysis of the development of the LCN during fracture repair. We identified significant increases in canalicular number density as bone repair progressed, whereas mean lacuna volume significantly decreases over this time period. This study illustrates the advantage of using multiple X-ray and classical histological imaging modalities to describe the formation and evolution of a new LCN in bone seen within the fracture callus.

Disclosures

The authors declare no conflict of interest.

Acknowledgements

The authors would like to thank Matthew Summers, Alyson Morse, and Kathy Mikulec for technical assistance. We acknowledge ETH Zurich and The Children's Hospital at Westmead for funding this study.

References

1. Jacobs CR, Temiyasathit S, Castillo AB. Osteocyte mechanobiology and pericellular mechanics. Annual review of biomedical engineering. Aug 15 2010;12:369-400.
2. Burra S, Nicolella DP, Francis WL, Freitas CJ, Mueschke NJ, Poole K, et al. Dendritic processes of osteocytes are mechanotransducers that induce the opening of hemichannels. P Natl Acad Sci USA. Aug 3 2010;107(31):13648-53.
3. Hesse B, Varga P, Langer M, Pacureanu A, Schrof S, Männicke N, et al. Canalicular Network Morphology Is the Major Determinant of the Spatial Distribution of Mass Density in Human Bone Tissue: Evidence by Means of Synchrotron Radiation Phase-Contrast nano-CT. Journal of Bone and Mineral Research. 2015;30(2):346-56.
4. Nango N, Kubota S, Hasegawa T, Yashiro W, Momose A, Matsuo K. Osteocyte-directed bone demineralization along canaliculi. Bone. 2015.
5. Wysolmerski JJ. Osteocytic osteolysis: time for a second look? Bonekey Rep. 2012;1:229.
6. Wysolmerski JJ. Osteocytes remove and replace perilacunar mineral during reproductive cycles. Bone. 2013;54(2):230-6.
7. Zarrinkalam MR, Mulaibrahimovic A, Atkins GJ, Moore RJ. Changes in osteocyte density correspond with changes in osteoblast and osteoclast activity in an osteoporotic sheep model. Osteoporosis international : a journal established as result of cooperation between the European Foundation for Osteoporosis and the National Osteoporosis Foundation of the USA. Apr 2012;23(4):1329-36.
8. Iwamoto J, Matsumoto H, Takeda T, Sato Y, Yeh JK. Effects of vitamin K2 on cortical and cancellous bone mass, cortical osteocyte and lacunar system, and porosity in sciatic neurectomized rats. Calcified tissue international. Sep 2010;87(3):254-62.
9. Qiu S, Rao DS, Palnitkar S, Parfitt AM. Reduced iliac cancellous osteocyte density in patients with osteoporotic vertebral fracture. Journal of bone and mineral research : the official journal of the American Society for Bone and Mineral Research. Sep 2003;18(9):1657-63.
10. Ma YL, Dai RC, Sheng ZF, Jin Y, Zhang YH, Fang LN, et al. Quantitative associations between osteocyte density and biomechanics, microcrack and microstructure in OVX rats vertebral trabeculae. J Biomech. 2008;41(6):1324-32.
11. Reilly GC. Observations of microdamage around osteocyte lacunae in bone. J Biomech. Sep 2000;33(9):1131-4.
12. Ma Y-L, Dai R-C, Sheng Z-F, Jin Y, Zhang Y-H, Fang L-N, et al. Quantitative associations between osteocyte density and biomechanics, microcrack and microstructure in OVX rats vertebral trabeculae. J Biomech. 2008;41(6):1324-32.
13. Qiu S, Rao DS, Fyhrie DP, Palnitkar S, Parfitt AM. The morphological association between microcracks and osteocyte lacunae in human cortical bone. Bone. 2005;37(1):10-5.
14. Currey JD, Shahar R. Cavities in the compact bone in tetrapods and fish and their effect on mechanical properties. Journal of structural biology. 2013;183(2):107-22.
15. Wagermaier W, Klaushofer K, Fratzl P. Fragility of bone material controlled by internal interfaces. Calcified tissue international. 2015;97(3):201-12.
16. Bonewald LF. Generation and function of osteocyte dendritic processes. Journal of musculoskeletal & neuronal interactions. Oct-Dec 2005;5(4):321-4.
17. Kerschnitzki M, Kollmannsberger P, Burghammer M, Duda GN, Weinkamer R, Wagermaier W, et al. Architecture of the osteocyte network correlates with bone material quality. Journal of bone and mineral research : the official journal of the American Society for Bone and Mineral Research. Aug 2013;28(8):1837-45.

18. Kerschnitzki M, Wagermaier W, Roschger P, Seto J, Shahar R, Duda GN, et al. The organization of the osteocyte network mirrors the extracellular matrix orientation in bone. J Struct Biol. Feb 2011;173(2):303-11.
19. Choy MHV, Wong RMY, Chow SKH, Li MC, Chim YN, Li TK, et al. How much do we know about the role of osteocytes in different phases of fracture healing? A systematic review. Journal of orthopaedic translation. Mar 2020;21:111-21. Epub 2020/04/21.
20. Hernandez CJ, Majeska RJ, Schaffler MB. Osteocyte density in woven bone. Bone. Nov 2004;35(5):1095-9.
21. Cardoso L, Fritton SP, Gailani G, Benalla M, Cowin SC. Advances in assessment of bone porosity, permeability and interstitial fluid flow. J Biomech. 2013;46(2):253-65.
22. Casanova M, Herelle J, Thomas M, Softley R, Schindeler A, Little D, et al. Effect of combined treatment with zoledronic acid and parathyroid hormone on mouse bone callus structure and composition. Bone. Nov 2016;92:70-8. Epub 2016/08/21.
23. Qiu S, Rao DS, Palnitkar S, Parfitt AM. Relationships between osteocyte density and bone formation rate in human cancellous bone. Bone. Dec 2002;31(6):709-11.
24. Vashishth D, Gibson G, Kimura J, Schaffler M, Fyhrie D. Determination of bone volume by osteocyte population. The Anatomical Record. 2002;267(4):292-5.
25. Metz LN, Martin RB, Turner AS. Histomorphometric analysis of the effects of osteocyte density on osteonal morphology and remodeling. Bone. 2003;33(5):753-9.
26. Cardoso L, Herman BC, Verborgt O, Laudier D, Majeska RJ, Schaffler MB. Osteocyte apoptosis controls activation of intracortical resorption in response to bone fatigue. Journal of bone and mineral research. 2009;24(4):597-605.
27. Webster DJ, Schneider P, Dallas SL, Muller R. Studying osteocytes within their environment. Bone. Jun 2013;54(2):285-95.
28. M Casanova AS, D Little. P Schneider, R Müller A novel method to quantify number of osteocyte processes in bone. European Society of Biomechanics Congress; Patras2013.
29. Schindeler A, Morse A, Harry L, Godfrey C, Mikulec K, McDonald M, et al. Models of tibial fracture healing in normal and Nf1-deficient mice. J Orthop Res. Aug 2008;26(8):1053-60. Epub 2008/04/03.
30. Bouxsein ML, Boyd SK, Christiansen BA, Guldberg RE, Jepsen KJ, Muller R. Guidelines for assessment of bone microstructure in rodents using micro-computed tomography. Journal of bone and mineral research : the official journal of the American Society for Bone and Mineral Research. Review Jul 2010;25(7):1468-86.
31. Wehrle E, Tourolle Né Betts DC, Kuhn GA, Scheuren AC, Hofmann S, Müller R. Evaluation of longitudinal time-lapsed in vivo for monitoring fracture healing in mouse femur defect models. Scientific reports. Nov 25 2019;9(1):17445. Epub 2019/11/27.
32. Bissinger O, Götz C, Wolff KD, Hapfelmeier A, Prodinger PM, Tischer T. Fully automated segmentation of callus by compared to biomechanics. Journal of orthopaedic surgery and research. Jul 11 2017;12(1):108. Epub 2017/07/13.
33. Macdonald W, Shefelbine SJ. Characterising neovascularisation in fracture healing with laser Doppler and scanning. Medical & biological engineering & computing. Oct 2013;51(10):1157-65. Epub 2013/07/25.
34. Pazzaglia UE, Congiu T. The cast imaging of the osteon lacunar-canalicular system and the implications with functional models of intracanalicular flow. Journal of anatomy. 2013;222(2):193-202.
35. Lau KW, Rundle CH, Zhou XD, Baylink DJ, Sheng MH. Conditional deletion of IGF-I in osteocytes unexpectedly accelerates bony union of the fracture gap in mice. Bone. Nov 2016;92:18-28. Epub 2016/08/16.

36. Dallas SL, Xie Y, Shiflett LA, Ueki Y. Mouse Cre Models for the Study of Bone Diseases. Current osteoporosis reports. Aug 2018;16(4):466-77. Epub 2018/06/24.
37. Inoue K, Mikuni-Takagaki Y, Oikawa K, Itoh T, Inada M, Noguchi T, et al. A crucial role for matrix metalloproteinase 2 in osteocytic canalicular formation and bone metabolism. The Journal of biological chemistry. Nov 3 2006;281(44):33814-24. Epub 2006/09/09.
38. Lieu S, Hansen E, Dedini R, Behonick D, Werb Z, Miclau T, et al. Impaired remodeling phase of fracture repair in the absence of matrix metalloproteinase-2. Disease models & mechanisms. Mar 2011;4(2):203-11. Epub 2010/12/08.
39. Colnot C, Thompson Z, Miclau T, Werb Z, Helms JA. Altered fracture repair in the absence of MMP9. Development. 2003 Sep;130(17):4123-33.
40. Tang SY, Herber R-P, Ho SP, Alliston T. Matrix metalloproteinase-13 is required for osteocytic perilacunar remodeling and maintains bone fracture resistance. J Bone Miner Res. 2012 Sep; 27(9):1936-1950.

Author Contribution Statement: MC was the lead investigator and performed microCT and high resolution microscopy, LP undertook the animal studies, LL performed histology, PS contributed to microCT analysis, MC and AS drafted the manuscript, AS, DGL and RM conceived and planned the study, all authors edited and reviewed the final manuscript.

Table 1 Quantitative micro-computed tomography macro-/microarchitecture, lacunar occupancy and tissue mineral density of the bone calluses (new bone) and intact tibiae. Ca.D: canalicular number density; <Lc.V>: mean lacuna volume; N.Lc/BV: lacunar number density; BV/TV: bone volume fraction; TMD: tissue mineral density; Tb.N: trabecular number; Tb.Th: trabecular thickness; Tb.Sp: trabecular separation; Tb.Th.SD: standard deviation of Tb.Th; Tb.Sp.SD: standard deviation of Tb.Sp; DA: degree of anisotropy; Conn.D: connectivity density; SMI: structure model index. Parenthetic numbers indicate standard deviation.

	2 weeks post-op	**3 weeks post-op**	**6 weeks post-op**
Lacunar and canalicular measures			
Bone calluses	*N=15*	*N=15*	*N=15*
Ca.D (1/μm²)	0.082 (0.021)	0.10 (0.033)*	0.151 (0.033)***,###
<Lc.V> (μm³)	501 (99)	366 (29)***	319 (27)***,#
N.Lc/BV (10^3/mm³)	20.4 (4.3)	52.4 (11.5)***	42.9 (7.5)***, #
	N=5	N=5	N=5
Lacunar occupancy (%)	94 (3.5)	94 (2.8)	94 (1.5)
Intact tibiae	*N=15*	*N=15*	*N=15*
Ca.D (1/μm²)	0.179 (0.035)	0.175 (0.034)	0.182 (0.039)
<Lc.V> (μm³)	302 (34)	297 (29)	312 (26)
N.Lc/BV (10^3/mm³)	52.7 (13.4)	44.9 (11.7)	47 (11.5)
	N=5	N=5	N=5
Lacunar occupancy (%)	93 (3.2)	92 (0.9)	90 (3.9)
Macroscopic measures			
Bone calluses	*N=15*	*N=15*	*N=15*
BV/TV (%)	36.5 (6.0)	43.9 (8.4)*	37.3 (9.6)
TMD (HA mg/cm³)	627 (44)	796 (26)***	920 (24)***,###
Micro-architectural measures			
Bone calluses	*N=15*	*N=15*	*N=14*
Tb.N (1/mm)	12.8 (1.6)	7.8 (1.5)***	3.3 (0.7)***,###
Tb.Th (mm)	0.034 (0.0025)	0.049 (0.0053)***	0.085 (0.0159)***,###
Tb.Sp (mm)	0.072 (0.0129)	0.124 (0.0251)***	0.300 (0.0526)***,###
Tb.Th.SD (mm)	0.0121 (0.0016)	0.0196 (0.0058)*	0.0386 (0.0117)***,###
Tb.Sp.SD (mm)	0.479 (0.020)	0.072 (0.024)*	0.130 (0.031)***,###
DA (-)	1.059 (0.014)	1.213 (0.081)***	1.543 (0.140)***,###
Conn.D (1/mm³)	3753 (524)	1537 (378)***	93 (58)***,###
SMI (-)	0.895 (0.350)	0.484 (0.659)	1.870 (0.756)***,###

*: $p < 0.05$ when compared to 2 weeks post-op
**: $p < 0.01$ when compared to 2 weeks post-op
***: $p < 0.001$ when compared to 2 weeks post-op
#: $p < 0.05$ when compared to 3 weeks post-op
###: $p < 0.001$ when compared to 3 weeks post-op

Table 2 Statistically significant Pearson correlations between micro-architectural measures and lacuno-canalicular measures. SMI: structure model index; Ca.D: canalicular number density; DA: degree of anisotropy; Lc.D: lacunar number density; Tb.N: trabecular number; Tb.Sp: trabecular spacing; Tb.Th.SD: standard deviation of Tb.Th; Conn.D: connectivity density; Post-op week: post-operative week.

	Tb.Th.SD~ Lc.D	**DA~ Lc.D**	**Tb.N~ Ca.D**	**Tb.Sp~ Ca.D**	**Conn.D~ Ca.D**	**SMI~ Ca.D**
	N=15	*N=15*	*N=15*	*N=15*	*N=15*	*N=14*
Post-op week	2	3	3	3	3	6
Pearson's *R*	0.738	0.708	0.709	-0.808	0.753	0.706
p-value	0.006	0.003	0.003	0.000	0.001	0.003

Figure Legends

Figure 1: Three-dimensional rendering of representative calluses (scans at 7 μm voxel size) for each time point (top). Representative details of the callus struts from the transverse plane (scans at 1.2 μm voxel size) at the three post-operative (post-op) time points; acquired in the white rectangular area on the top images (bottom).

Figure 2: Trabecular thickness versus canalicular number density or lacunar volume for all calluses of the three time points: two, three and six weeks post-operatively. A significant linear correlation of R^2=0.56 ($p < 0.001$) was found for canalicular number density, and a significant quadratic correlation of R^2=0.57 ($p < 0.001$) was found for mean lacuna volume.

Figure 3: Illustrative images of canaliculi in the calluses at the three different time points. The yellow area delimits the lacunar contour (ROI). (A) Microscopy sections cutting through the centre of the lacunae. (B) Confocal planes placed a few micrometres above the lacunae.

Figure 4: TUNEL staining of fracture calluses (top row) with 40× magnified regions below (boxed) corresponding to the callus tissue (middle row) and parosteal cortical bone adjacent to the callus (bottom row). TUNEL staining (brown), haematoxylin counterstain (purple).

Figure 5: Descriptive histology with Goldner's trichrome staining showing lacunar occupancy in the woven bone of (a) the bone callus, (b) the cortical bone of the intact tibia, and (c) on the reabsorbing cortical bone in the bone callus.

Figure 6: Tissue mineral density (TMD) of the necrotic bone in the bone calluses (fractured tibiae) compared to the TMD of the intact tibiae showed no significant difference. However, the mean lacuna volume of necrotic (dead) old cortical bone was significantly higher than other bone at the 2 and 3 week time points. Bars represent standard deviation. *: $p < 0.05$; **: $p < 0.01$.

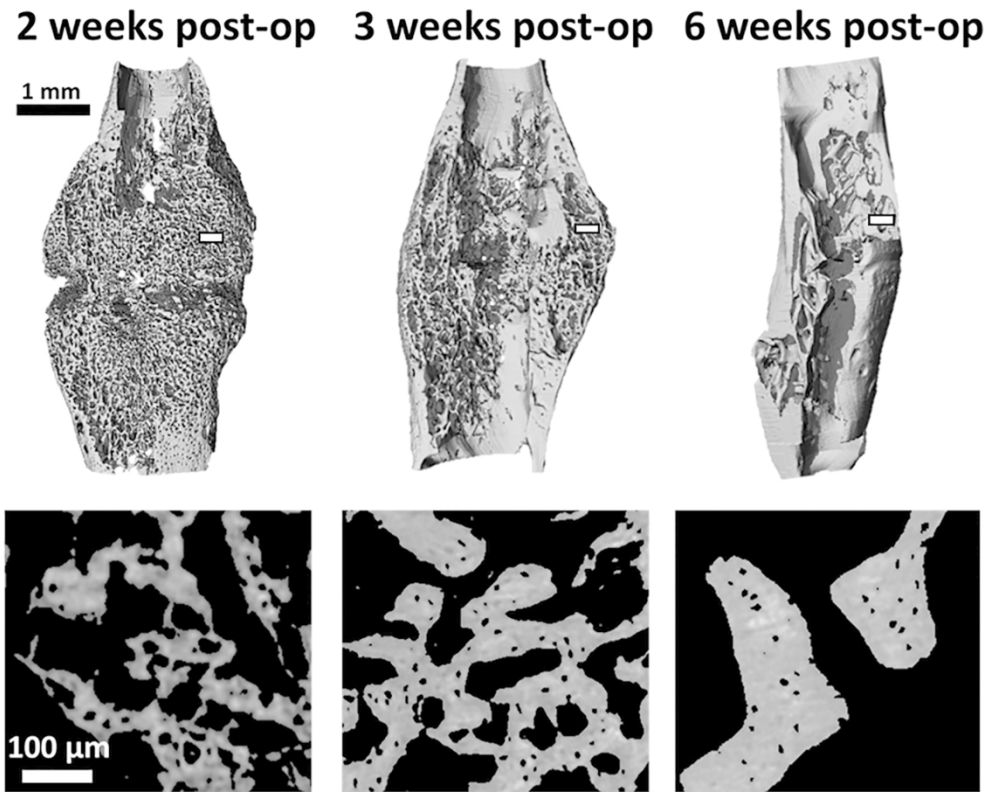

Figure 1: Three-dimensional rendering of representative calluses (scans with 7 µm voxel size) for each time point (top). Representative details of the callus struts from the transverse plane (scans with 1.2 µm voxel size) at the three post-operative (post-op) time points; acquired in the white rectangular area on the top images (bottom).

182x146mm (300 x 300 DPI)

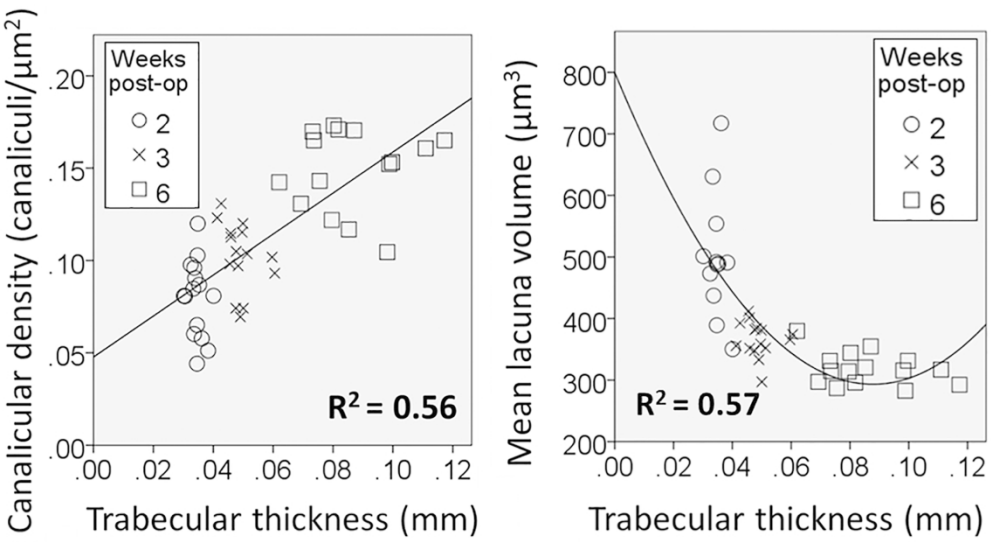

Figure 2: Trabecular thickness versus canalicular density or lacunar volume for all calluses of the three time points: two, three and six weeks post-operatively. A significant linear correlation of R2=0.56 ($p < 0.001$) was found for canalicular density, and a significant quadratic correlation of R2=0.57 ($p < 0.001$) was found for mean lacunar volume.

182x99mm (300 x 300 DPI)

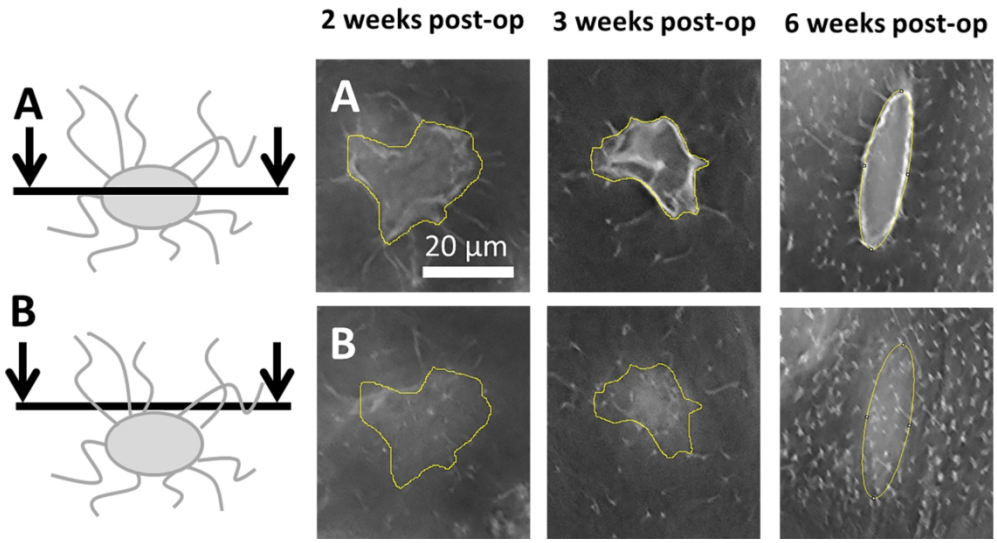

Figure 3: Illustrative images of canaliculi in the calluses in the three different time points. The yellow area delimits the lacunar contour (ROI). (A) Microscopy sections cutting through the centre of the lacunae. (B) Confocal planes placed a few micrometres above the lacunae.

182x96mm (300 x 300 DPI)

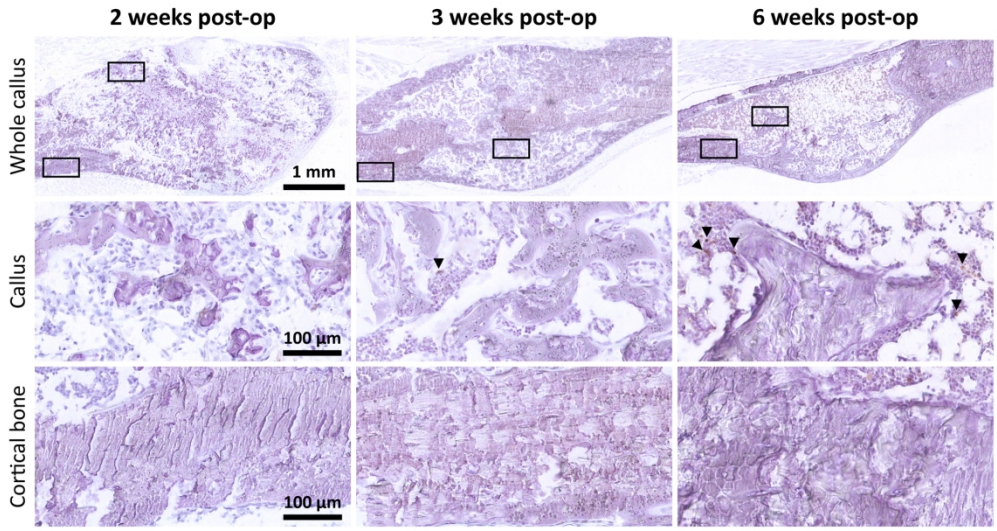

Figure 4: TUNEL staining of fracture calluses (top row) with 40× magnified regions below (boxed) corresponding to the callus tissue (middle row) and parosteal cortical bone adjacent to the callus (bottom row). TUNEL staining (brown), haematoxylin counterstain (purple).

182x96mm (300 x 300 DPI)

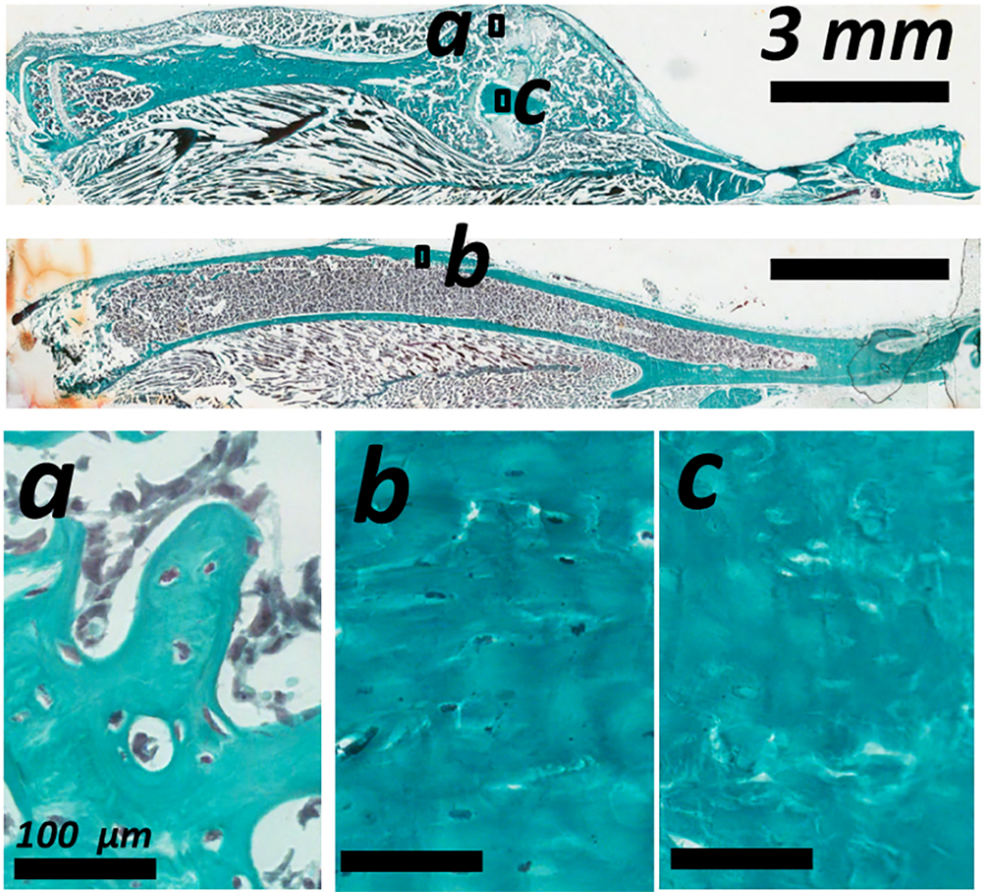

Figure 5: Descriptive histology with Goldner's trichrome staining showing lacunar occupancy in the woven bone of (a) the bone callus, (b) the cortical bone of the intact tibia, and (c) on the reabsorbing cortical bone in the bone callus.

86x77mm (300 x 300 DPI)

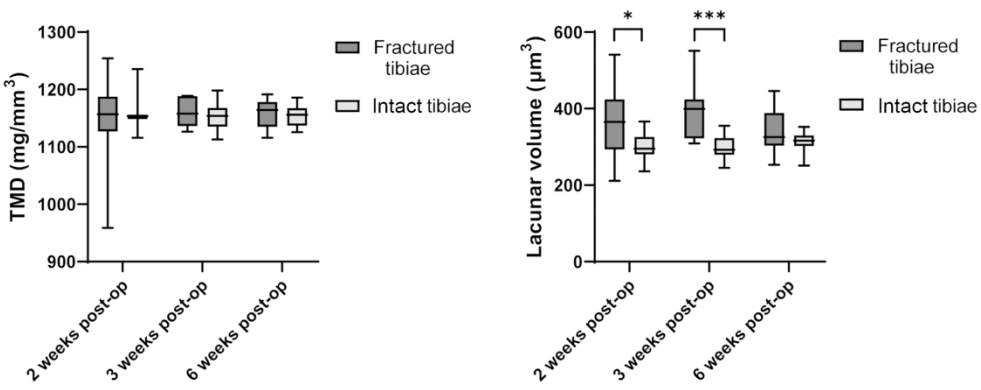

Figure 6: Tissue mineral density (TMD) of the necrotic bone in the bone calluses (fractured tibiae) compared to the TMD of the intact tibiae showed no significant difference. However, the mean lacunar volume of necrotic (dead) old cortical bone was significantly higher than other bone at the 2 and 3 week time points. Bars represent SD. *: $p < 0.05$; **: $p < 0.01$)